# Preparation, Structural Characterization, Assessment of Potential Antiaromaticity and Metalation of 21-Oxyazuliporphyrins

Timothy D. Lash,* Denise A. Colby, Jessica A. El-Beck, Deyaa I. AbuSalim, and Gregory M. Ferrence

Department of Chemistry, Illinois State University, Normal, Illinois 61790-4160, United States

S *Supporting Information*

ABSTRACT: Oxidation of tetraarylazuliporphyrins with silver(I) acetate in refluxing chloroform—acetonitrile afforded good yields of 21-oxyazuliporphyrins. Although hydroxyazuliporphyrin tautomers can be considered for this system, spectroscopic results and density functional theory calculations indicate that the keto form is favored, and this was confirmed by single-crystal X-ray diffraction. Oxyazuliporphyrins formally possess a 24π electron delocalization pathway, but the proton NMR spectra are consistent with macrocycles that have diatropic ring currents. Nucleus independent chemical shift and anisotropy of induced current density calculations also confirmed the diatropic nature of these macrocycles, although these results indicated that the seven-membered ring is antiaromatic. However, while the NMR spectra showed the azulene protons at atypically high field values, the results are consistent with a nonaromatic cycloheptatrienyl unit. Protonation gave dicationic products that exhibited enhanced diatropic character. Oxyazuliporphyrins readily form metalated derivatives with Ni(II), Pd(II), and Pt(II), and these complexes exhibited significant diatropic character even though the macrocycle is highly distorted. X-ray diffraction characterization of palladium(II) and platinum(II) complexes demonstrated that these derivatives are structurally virtually identical to a previously reported copper(II) oxyazuliporphyrin.

M = Ni, Pd or Pt
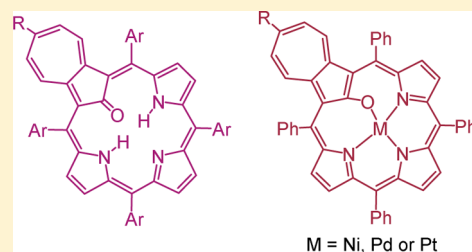
INTRODUCTION

Following the discovery of N-confused porphyrins **1** in 1994,[1] numerous classes of carbaporphyrinoid systems have been

1
N-Confused Porphyrin

2
Benziporphyrin

3
Oxybenziporphyrin

4
Benzocarbaporphyrin

5
Tropiporphyrin

6
Azuliporphyrin
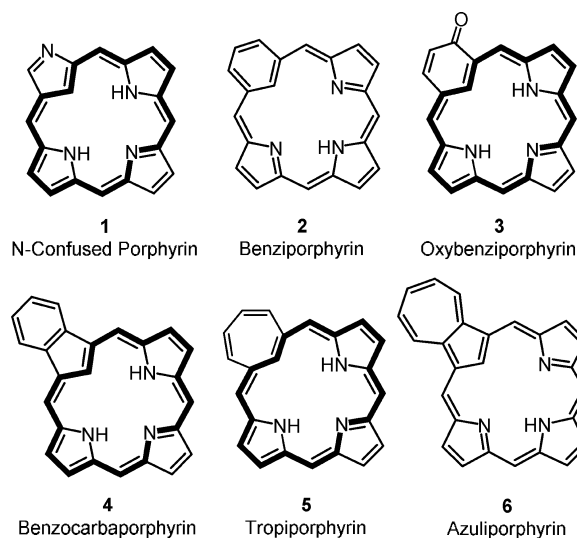
investigated[2,3] including benziporphyrins **2**,[4] oxybenziporphyrins **3**,[5] carbaporphyrins such as **4**,[6] tropiporphyrins **5**,[7] and azuliporphyrins **6**.[8] Replacement of one of the nitrogens within the porphyrinoid cavity with a carbon atom clearly has a profound impact on the ability of these structures to undergo metalation reactions. Nevertheless, these systems have been reported to give a wide range of stable organometallic
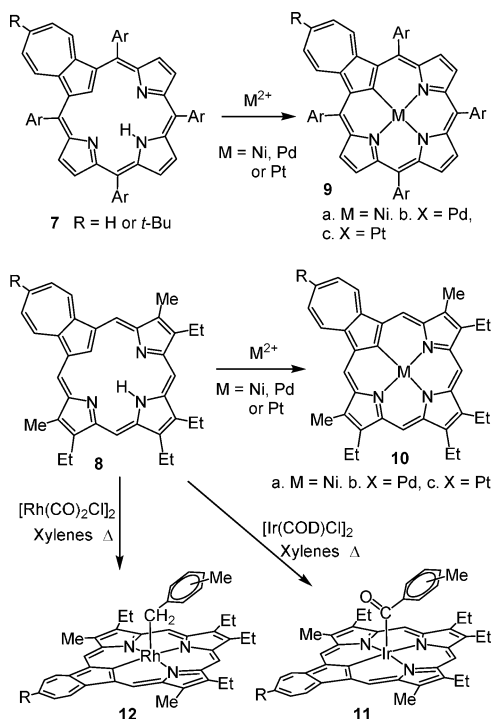
derivatives.[9] The metalation of N-confused porphyrins has been particularly well-studied,[10−12] but many examples of metalated benziporphyrins,[13] oxybenziporphyrins,[14] carbaporphyrins,[15] tropiporphyrins,[7] and related systems[16] have also been reported. Azuliporphyrins are a particularly interesting family of carbaporphyrinoids that possess an azulene subunit within a porphyrin-like framework.[8,17] Azuliporphyrins are formally cross-conjugated but still retain a degree of diatropic character. The proton NMR spectra of azuliporphyrins typically show the internal CH resonance near 3 ppm,[17] which is ~5 ppm upfield compared to the resonance for the equivalent proton in azulene, while the external *meso*-protons appear in a relatively downfield region between 8 and 9 ppm.[8,17,18] Protonation leads to a substantial enhancement of the aromatic ring current.[8,17] Azuliporphyrins also have unique reactivity, undergoing an oxidative ring contraction with peroxides under basic conditions to afford benzocarbaporphyrin products[19] and readily forming organometallic derivatives.[20−23] Three synthetic routes to *meso*-unsubstituted azuliporphyrins have been developed,[8,24,25] and a one-pot synthesis of tetraarylazuliporphyrins from azulene, pyrrole, and aromatic aldehydes has also been reported.[26−28] The latter approach typically affords 10—20% yields of azuliporphyrins and makes this system easily accessible. In early studies, tetraarylazuliporphyrins **7** and *meso*-unsubstituted azuliporphyrins **8** were shown to react with nickel(II) acetate, palladium(II) acetate, or platinum(II)

Scheme 1. Metalation of Azuliporphyrins
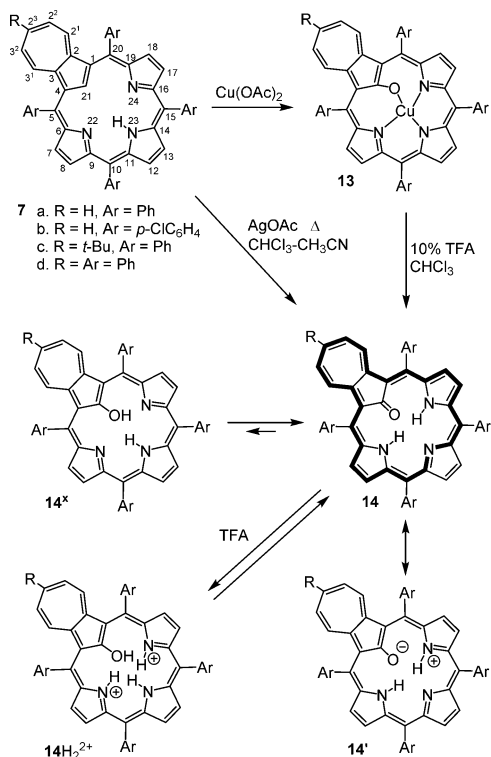

7   R = H or *t*-Bu

9
a. M = Ni. b. X = Pd,
c. X = Pt

8

10
a. M = Ni. b. X = Pd, c. X = Pt

[Rh(CO)₂Cl]₂
Xylenes Δ

[Ir(COD)Cl]₂
Xylenes Δ

12

11

Scheme 2. Synthesis, Tautomerization, and Protonation of 21-Oxyazuliporphyrins

7   a. R = H, Ar = Ph
b. R = H, Ar = *p*-ClC₆H₄
c. R = *t*-Bu, Ar = Ph
d. R = Ar = Ph

13

Cu(OAc)₂

AgOAc Δ
CHCl₃-CH₃CN

10% TFA
CHCl₃

14x

14

TFA

14H₂²⁺

14'

chloride to give the corresponding organometallic derivatives **9** and **10**, respectively (Scheme 1).[20,21] These metallo-azuliporphyrins proved to be very stable compounds and retained moderate aromatic characteristics. Recently, azuliporphyrins **8** were shown to react with [Ir(COD)Cl]₂ in refluxing xylenes to give low yields of benzoyliridium(III) azuliporphyrins **11**,[22]

while [Rh(CO)₂Cl]₂ reacted with **8** to give similar benzylic rhodium(III) porphyrinoids **12** (Scheme 1).[23] In addition, the formation of ruthenium complexes of azuliporphyrins has also been disclosed.[29] When tetraphenylazuliporphyrin **7a** was reacted with copper(II) acetate in pyridine, an unexpected oxymetalation reaction took place to give copper(II) complex **13a** in 30% yield rather than the expected copper(II) azuliporphyrin (Scheme 2).[30] Tetrakis(4-chlorophenyl)-azuliporphyrin **7b** similarly afforded the related complex **13b** in 16% yield. Demetalation of **13a** with 10% trifluoroacetic acid (TFA) in chloroform gave the related free base structure **14a**, which we named 21-oxyazuliporphyrin.[30] The reaction with copper(II) acetate was performed under nitrogen, but labeling studies with ¹⁸O₂ demonstrated that the oxygen atom in **13** and **14** originated from molecular oxygen.[30] 21-Oxyazuliporphyrin was assigned as the keto tautomer **14** rather than the 21-hydroxyazulene structure **14ˣ**. Very recently, examples of ruthenium(II) complexes related to **13** were reported.[31] In this study, the parent tetraphenyl-21-oxyazuliporphyrin **14a** was represented as the hydroxy tautomer **14ˣ**, although no evidence for this assignment was presented. In this paper, an improved synthesis of 21-oxyazuliporphyrins is reported, and **14a** has been structurally characterized for the first time by X-ray diffraction (XRD). The identity of the favored tautomer is firmly established using spectroscopic characterization, density functional theory (DFT) calculations, and the XRD results. In addition, the ability of 21-oxyazuliporphyrins to act as a ligand was investigated, and Ni(II), Pd(II), and Pt(II) complexes were prepared.

RESULTS AND DISCUSSION

Reaction of tetraarylazuliporphyrins **7** with copper(II) acetate gave relatively low yields of copper(II) complex **13**, and even though demetalation with TFA-chloroform gave good to excellent results, the overall yields of oxyazuliporphyrins **14** were poor. Subsequent to the initial study, it was discovered that superior yields of **14** could be obtained by treating **7** with 2 equiv of silver(I) acetate in refluxing chloroform—acetonitrile (Scheme 2). Azuliporphyrin **7a** reacted under these conditions, and following purification by column chromatography and recrystallization from chloroform—methanol, the related oxyazuliporphyrin **14a** was isolated in 54% yield. These reaction conditions also gave good results for the conversion of **7b**−**7d** into **14b**−**14d**. Similar oxidation reactions have been reported for benziporphyrins,[32,33] pyriphlorins,[34] and a dicarbaporphyrinoid system.[35] This improved synthesis of 21-oxyazuliporphyrins has facilitated further investigations into this interesting porphyrinoid system. Oxyazuliporphyrin **14a** gives a surprisingly porphyrin-like UV−vis spectrum with a strong Soret band at 520 nm and several Q bands at higher wavelengths (Figure 1).[36] If this compound favors the keto-tautomer **14**, it can be envisaged that the macrocycle could take on antiaromatic characteristics due to the presence of a 24π electron delocalization pathway (highlighted in bold). However, the UV−vis spectrum is not consistent with this type of system, and in any case the macrocycle would not be expected to have a planar geometry. The UV−vis spectra for **14b**−**d** were very similar. The Soret-like band for *tert*-butylazuliporphyrin **14c** was shifted to 525 nm, while the pentaphenylazuliporphyrin **14d** gave this absorption at a further bathochromically shifted value of 533 nm. In the latter case, the longest wavelength Q-band was shifted to 730 nm, compared to 715 nm for **14a**. These shifts may be due in part to conjugation between the 2³-
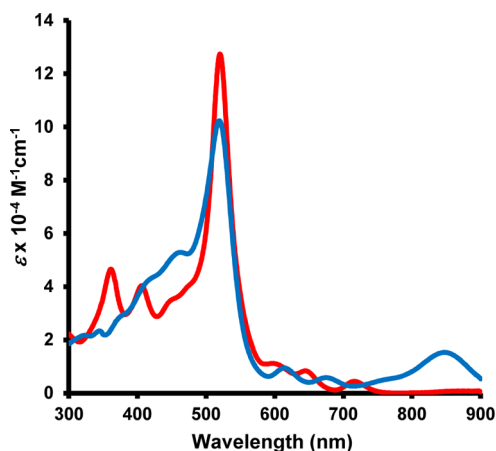
Figure 1. UV−vis spectra of 21-oxyazuliporphyrin **14a** in 1% triethylamine−dichloromethane (red line, free base) and 1% TFA−dichloromethane (blue line, dication **14H$_2$$^{2+}$**).

phenyl substituent and the porphyrinoid. The proton NMR spectra of 21-oxyazuliporphyrins are particularly insightful. For **14a** in CDCl$_3$ (Figure 2), the azulene protons show up at unusually upfield values of 5.16 (2H, d), 5.37 (1H, t) and 5.68 (2H, t). In tetraphenylazuliporphyrin **7a**, these resonances appear at typically aromatic values of 6.92, 7.25, and 7.64 ppm, and the results for **14a** suggest that the seven-membered ring has olefinic characteristics but do not indicate the presence of a paratropic ring current. However, the pyrrolic protons in **14a** gave resonances at 7.38 (2H, d), 7.52 (2H, s), and 7.84 ppm (2H, d), values that are similar to those seen in **7a** and which are consistent with the presence of a moderate diatropic ring current. This contrasts to nonaromatic tetraphenylbenziporphyrin, which gave signals for the analogous pyrrolic protons comparatively upfield between 6.5 and 7.2 ppm.[32,33] These results are not consistent with a hydroxyazulene tautomer like **14^x** because the azulene protons would appear in the aromatic region for a structure of this type, but further evidence was required to firmly establish the identity of the favored tautomer. The proton NMR results for **14b−d** were similar, although **14c** and **14d** gave rise to two 2H doublets for the azulene ring. The presence of 4-chlorophenyl substituents led to a small upfield shift to the pyrrolic protons, while the azulene protons underwent a small but noticeable downfield shift. The carbon-13 NMR spectra for **14a−d** confirmed the presence of a plane of symmetry in these porphyrinoids. The appearance of a peak at 162.7 ppm is consistent with the presence of a

carbonyl moiety, although this value does not fall into the range expected for a ketone. In addition, as reported in the earlier study, the IR spectrum shows a strong absorption at 1524 cm$^{−1}$, a value that is very low for carbonyl stretching. This implies that the C=O bond is highly polarized due to dipolar canonical forms such as **14′** (Scheme 2), although strong hydrogen bonding to the NH's may also be a factor. The identities of **14a−d** were also confirmed by high-resolution mass spectrometry.

Addition of TFA to solutions of **14** gave rise to significant changes in the UV−vis spectra due to protonation. Titration with TFA indicated that several different species were formed (see Supporting Information), although it was anticipated that dication **14H$_2$$^{2+}$** was generated on addition of excess TFA. In 1% TFA−dichloromethane, **14a** gave a Soret-like band at 519 nm and several smaller absorptions at higher wavelengths including a broad band centered on 848 nm (Figure 1). The proton NMR spectra of **14a−d** in TFA-CDCl$_3$ were difficult to interpret due to overlap of many of the resonances in the aromatic region. For **14aH$_2$$^{2+}$**, the azulene protons shifted downfield to 7.25−7.30 ppm, and at least two of the pyrrolic protons appear downfield from 8 ppm. These results are consistent with an aromatic azuliporphyrin-like dication and indicate that a species like **14H$_2$$^{2+}$** must have been formed. The carbon-13 NMR spectrum showed some broadening, possibly due to steric crowding, and the most downfield resonance appeared at 150.4 ppm. The latter result indicates that a carbonyl unit is no longer present in the protonated species.

To gain further insight into oxyazuliporphyrins, DFT calculations[37] were performed on a series of possible tautomers. Initially, the unsubstituted porphyrinoid system was investigated, and four reasonable tautomers, namely, **15**, **15^w**, **15^x**, and **15^y**, were considered using DFT-B3LYP/6-311++G(d,p). Optimization of **15^x** led to a curious result where the OH proton transfers to a nitrogen atom and gives keto tautomer **15^w**. This enables the macrocyclic cavity to incorporate favorable hydrogen-bonding interactions. Hence, tautomer **15^x** can only exist under highly constrained conditions, and calculations could only be performed on **15**, **15^w**, and **15^y** (Table 1). To assess the relative energies, single point energy (SPE) calculations were performed on the minimized structures using M06-2X/6-311++G(d,p) and B3LYP-D/6-311++G-(d,p).[38,39] The relative energies obtained from the M06-2X and the B3LYP-D functionals were consistent with the trends calculated using the B3LYP functional. Tautomer **15^w** was shown to be between 7.23 and 7.93 kcal/mol higher in energy
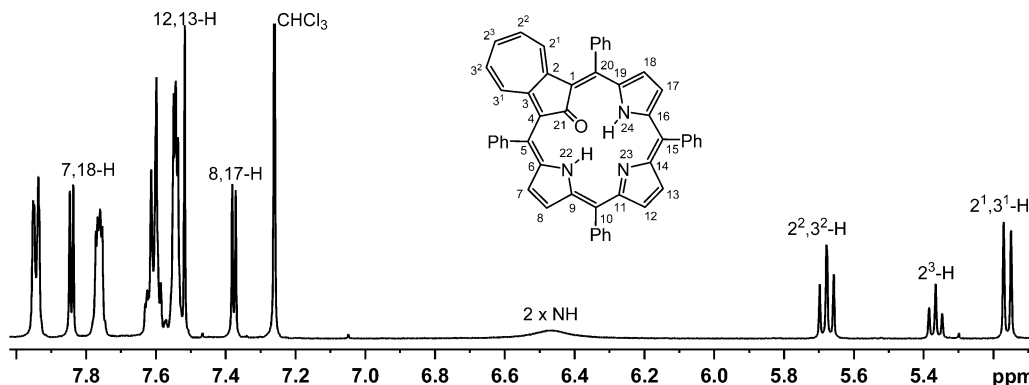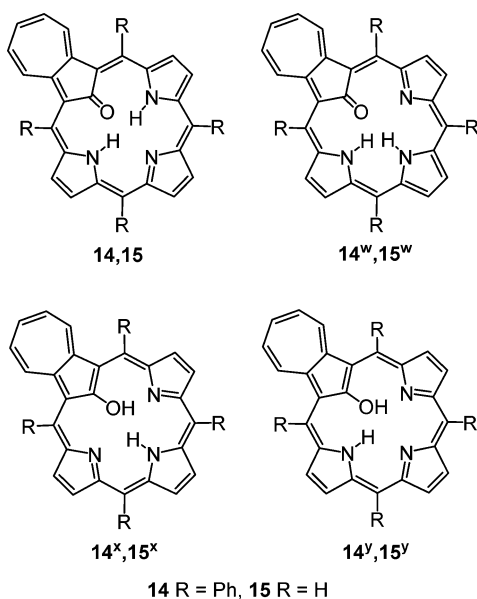

Figure 2. 500 MHz proton NMR spectrum of oxyazuliporphyrin **14a** in CDCl$_3$.

14,15　　　**14^w,15^w**

14^x,15^x　　　**14^y,15^y**
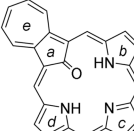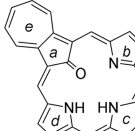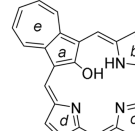
14 R = Ph, 15 R = H

than **15**, while hydroxy-tautomer **15^y** was ∼30 kcal/mol higher in energy. Comparable values were obtained for the relative ΔG values, indicating that no significant entropic factors are involved. In fact, all of the calculations performed gave similar ΔH and ΔG values, and for this reason only the ΔH results will be discussed below. Similar trends were seen for the tetraphenyl-substituted oxyazuliporphyrins **14**, **14^w**, and **14^y** (Table 1). In addition, tautomer **15^x** could not be analyzed because it converted to **15^w** during the optimization process in an analogous fashion to the observations noted for **14^x**. The aromatic character of these molecules was assessed using the GIAO method, which has commonly been used to probe porphyrinoid diatropic ring currents,[40−42] and nucleus independent chemical shifts (NICS) were used to assess the diatropic character of these species. NICS provides a measure of the theoretical upfield and downfield shifts at a given point within a structure, and strongly negative values can be correlated to aromatic character.[43] The standard NICS calculations include the effects of both σ- and π-electrons and must be interpreted with caution. NICS$_{zz}$ calculations provide an alternative method that can give more reliable insights into the aromatic character.[44] NICS$_{zz}$ calculations are commonly performed 1 Å above the ring (NICS(1)$_{zz}$) and mostly measure contributions from the π-system allowing the aromatic character to be more reliably assessed.[44−47] Both techniques were used in this study, and as has been noted for related systems the trends observed were similar for both types of calculations.[40] It is worth noting that the numerical values obtained using NICS$_{zz}$ are much larger than those calculated using NICS, and to avoid confusion only the latter values will be discussed. Structure **15** has a potential 24π electron delocalization pathway, and it was of some interest to see whether this structure possessed an overall paratropic ring current (paratropic systems give positive NICS values, whereas nonaromatic systems give results that are close to zero). It was therefore surprising to note that the NICS(0) value for **15** was calculated to be −5.24 ppm. This implies that the macrocycle has a moderate diatropic ring current and can be considered to be aromatic rather than antiaromatic. This is consistent with the observations made from the proton NMR spectra of tetraphenyloxyazuliporphyrins **14**, which show the pyrrolic protons at relatively downfield values. NICS values were also
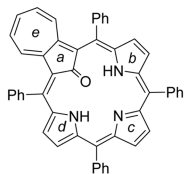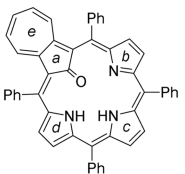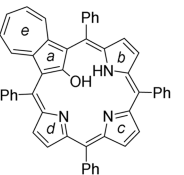
calculated for the individual rings, labeled *a−e* (Table 1). Rings *b* and *d* gave significantly negative values, but ring *c* was close to zero; ring *a* afforded a small positive value. More remarkably, ring *e* gave a value of +24.91 ppm, which is consistent with a paratropic ring current. Dipolar resonance contributors such as **15A** can be written for this structure that give the seven-membered ring antiaromatic character, although the data are more consistent with the macrocycle taking on a 19-atom 18π electron delocalization pathway of the type illustrated in structure **15B**. These results are mostly consistent with the proton NMR data for **14a−d**, although the protons on the seven-membered ring indicate that this unit is nonaromatic rather than paratropic. The NICS calculations for the less stable keto tautomer **15^w** were similar to those for **15**, although it is ring *b* in this case that has a very small NICS value; the favored delocalization pathway corresponds to structure **15C**. Hydroxyazulene tautomer **15^y** also gave an NICS(0) value that was consistent with a moderate diatropic ring current, but in this case ring *a* produced a surprisingly large negative NICS value of −13.33. These results imply that the 18π electron pathway shown in **15D** is favored for this tautomer. Calculations for tetraphenyl oxyazuliporphyrin tautomers **14** and **14^w** gave results similar to those for the corresponding unsubstituted porphyrinoids. Surprisingly, the overall diatropic ring current is slightly larger even though steric interactions involving the phenyl substituents result in a more distorted macrocyclic system. However, the paratropic characteristics of the seven-membered ring are much reduced, in line with experimental observations. The NICS(0) value for **14^y** is smaller than the result for **15^y**, and the conjugation pathway also appears to be modified in this case. Anisotropy of induced current density (AICD) plots also provide a valuable resource for the elucidation of favored conjugation pathways,[48] and computations of this type support the analyses discussed above for **14** and **15** (Figure 3). AICD plots are provided for all of the calculated structures in the Supporting Information section.

All of the structures investigated deviate significantly from planarity (Table 2). Keto tautomer **15** has dihedral angles between rings *a* and *b*, as well as for rings *d* and *e*, of 12.5°. These distortions are greatly magnified in the sterically crowded tetraphenyl substituted series, and the corresponding dihedral angles for **14a** were calculated to be 30.0° (Table 2). The calculated bond lengths for **14a** and **15** (Figure 4) indicate that there is a significant amount of aromatic character, particularly for the *meso*-unsubstituted system, and mostly support the delocalization pathway shown in structure **15B**. However, the bond lengths in ring *a* are relatively long implying that they have more single bond character. The C=O bond length was calculated to be 1.250 and 1.251 Å for **14a** and **15**, respectively, which falls into a typical range for carbonyl units. The very low value for carbonyl stretching that was observed in the IR spectra suggested that a weaker C=O bond was present. However, oxophlorins,[49] the keto tautomers of 5-hydroxyporphyrins, also give very low-frequency $\nu_{C=O}$ absorptions, but an X-ray crystallographic study demonstrated that the C=O bond length was 1.233 Å.[50] Hence, the calculated bond lengths are consistent with the observed spectroscopic properties for oxyazuliporphyrins.

As the protonation of **14a−d** gave complex results, DFT calculations were also performed on the monoprotonated and diprotonated forms of **14** and **15** (Table 3). In many cases, these species were even more distorted than the free base structures (Table 2) due to further crowding in the macrocyclic

Table 1. Calculated Relative Energies (kcal/mol) and NICS Values (ppm) for Oxyazuliporphyrin Tautomers

	15	15^w	15^y
Rel. ΔG	0.00	7.60	30.60
B3LYP/ **M06-2X/B3LYP-D**	0.00	7.93/ **7.23/7.93**	31.48/ **26.24/31.84**
NICS(0)/ **NICS(1)zz**	-5.24/ **-7.84**	-4.71/ **-7.58**	-6.20/ **-14.78**
NICS(a)/ **NICS (1a)zz**	+1.88/ **+1.84**	+2.56/ **+2.78**	-13.33/ **-25.00**
NICS(b)/ **NICS(1b)zz**	-7.44/ **-16.94**	-2.32/ **-10.78**	-7.42/ **-18.96**
NICS(c)/ **NICS(1c)zz**	-0.13/ **-5.85**	-6.22/ **-13.75**	-0.78/ **-6.63**
NICS(d)/ **NICS(1d)zz**	-7.44/ **-16.94**	-8.28/ **-17.64**	-0.39/ **-7.79**
NICS(e)/ **NICS(1e)zz**	+24.91/ **+56.32**	+21.92/ **+49.02**	+3.28/ **+10.62**

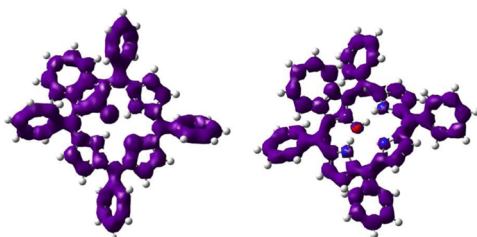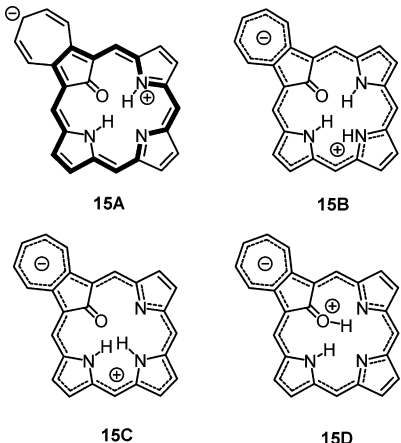|	14	14^w	14^y
Rel. ΔG	0.00	5.81	21.17
B3LYP/ **M06-2X/B3LYP-D**	0.00	5.47/ **5.06/5.39**	21.29/ **16.05/21.97**
NICS(0)/ **NICS(1)zz**	-6.46/ **-11.47**	-6.31/ **-9.88**	-4.14/ **-6.62**
NICS(a)/ **NICS (1a)zz**	-0.57/ **+9.52**	-1.61/ **+5.19**	-14.85/ **-19.22**
NICS(b)/ **NICS(1b)zz**	-7.10/ **-13.25**	-1.97/ **-5.03**	-6.03/ **-9.62**
NICS(c)/ **NICS(1c)zz**	-0.25/ **-8.07**	-7.18/ **-20.68**	-0.51/ **-11.41**
NICS(d)/ **NICS(1d)zz**	-7.10/ **-13.25**	-7.45/ **-15.63**	-1.66/ **-5.91**
NICS(e)/ **NICS(1e)zz**	+13.38/ **+31.88**	+8.91/ **+21.07**	-2.60/ **-6.44**

Figure 3. AICD plots of tetraphenyl-21-oxyazuliporphyrin **14a** (left) and the related dication **14aH$_2^{2+}$** (right) giving an indication of the favored delocalization pathways in these compounds. For these figures, the isosurface values were set at 0.06 and 0.07, respectively.

cavity. Three monocations were considered in each case, as well as the likely dicationic structures. For the unsubstituted series, keto tautomer **15H$^+$** (Table 3) proved to be the most stable form. The two hydroxy tautomers were between 12 and 24 kcal/mol higher in energy. Similar results were obtained for the tetraphenyl series, although the differences in energy were not as large (Table 3). **15H$^+$** gave a fairly large NICS(0) value, indicating the presence of a diatropic ring current. Rings b, c, and d also gave quite large negative values, although the seven-membered ring gave an NICS(e) value of +14.36, and ring a gave a smaller positive value (Table 3). The results are consistent with the delocalization pathway shown in structure **16A**, although this does not explain the NICS(a) value for the five-membered carbocyclic ring. It is possible that the polarized carbonyl group gives the five-membered ring antiaromatic cyclopentadienyl cationic character. Hydroxytautomers **15^{x}H$^+$** and **15^{y}H$^+$** both exhibit strong diatropic ring currents, and the individual NICS values for **15^{x}H$^+$** suggest that the favored delocalization pathway involves the 18π electron delocalization pathway shown in structure **16B**. The favored tetraphenyl tautomer **14H$^+$** (Table 3) gave similar results to **15H$^+$**, although the diatropic ring current is reduced. Tautomers **14^{x}H$^+$** and **14^{y}H$^+$** were also similar to their unsubstituted analogues; however, the seven-membered ring takes on weakly diatropic

Table 2. Dihedral Angles for 21-Oxyazuliporphyrin Tautomers and Related Protonated Species

15A   15B

15C   15D

molecule	dihedral ab	dihedral bc	dihedral cd	dihedral de	mean absolute dihedral
15	12.5	4.3	−4.3	−12.5	8.4
15^w	−20.4	2.9	7.6	9.8	10.2
15^y	−26.6	1.3	−5.4	27.9	15.3
15H$^+$	5.1	11.6	−11.6	−5.1	8.4
15^{y}H$^+$	26.2	−4.1	7.8	−27.6	16.4
15^{x}H$^+$	20.6	1.8	2.6	−23.4	12.1
15H$_2$$^{2+}$	28.1	−12.8	13.3	−26.9	20.3
14a	−30.0	8.6	−8.6	30.0	19.3
14^w	−40.4	19.2	−7.9	27.5	23.8
14^y	−42.7	16.0	−28.1	47.8	33.7
14H$^+$	−10.5	26.2	−26.2	10.5	18.4
14^{y}H$^+$	46.5	−22.1	23.4	−45.0	34.3
14^{x}H$^+$	40.5	−14.8	−31.9	49.1	34.1
14H$_2$$^{2+}$	−46.8	30.8	−31.9	49.1	39.7

characteristics for these species, and the NICS(0) values are reduced. Dication **15H$_2$$^{2+}$** gave an NICS(0) value of −11.71, indicating that this species is strongly diatropic. Rings *b*, *c*, and *d* all showed NICS values between −10 and −12, while ring *e* gave a value of −6.41; only ring *a* appeared to have little or no aromatic character. These results are consistent with the 19-atom 18π electron delocalization pathway shown in structure **17A**. Dication **14H$_2$$^{2+}$** gave somewhat different results and produced a lower NICS(0) value of −7.79. Importantly, ring *a* now shows a substantial NICS value of −9.11, implying that the delocalization pathway has been relocated through the periphery of this unit, as shown for structure **17B**. This pathway can also be visualized in an AICD plot (see Figure 3).

Further evidence for the nature of the oxyazuliporphyrin system was obtained from single-crystal XRD (Figure 5). The results demonstrate that free base **14a** is the keto-tautomer with the heteroatom attached hydrogen atoms being clearly identified in the difference Fourier to be connected to the pyrrolic nitrogen atoms N22 and N24, which are adjacent to the oxyazulenyl moiety. The 1.268(3) Å C21−O25 bond length is somewhat long for organic carbonyls, 0.037 Å longer than had been predicted by the DFT calculations, but was found by *Mogul* to be within two standard deviations of the 1.230 ± 0.020 Å average distance observed for carbonyls in a similar local environment. This is in contrast to the structure of tetraphenyl-21-hydroxy-N-confused porphyrin where the hydroxyl tautomer prevails and the observed C−O bond distance of 1.497(4) Å is consistent with the single bond assignment.[51]
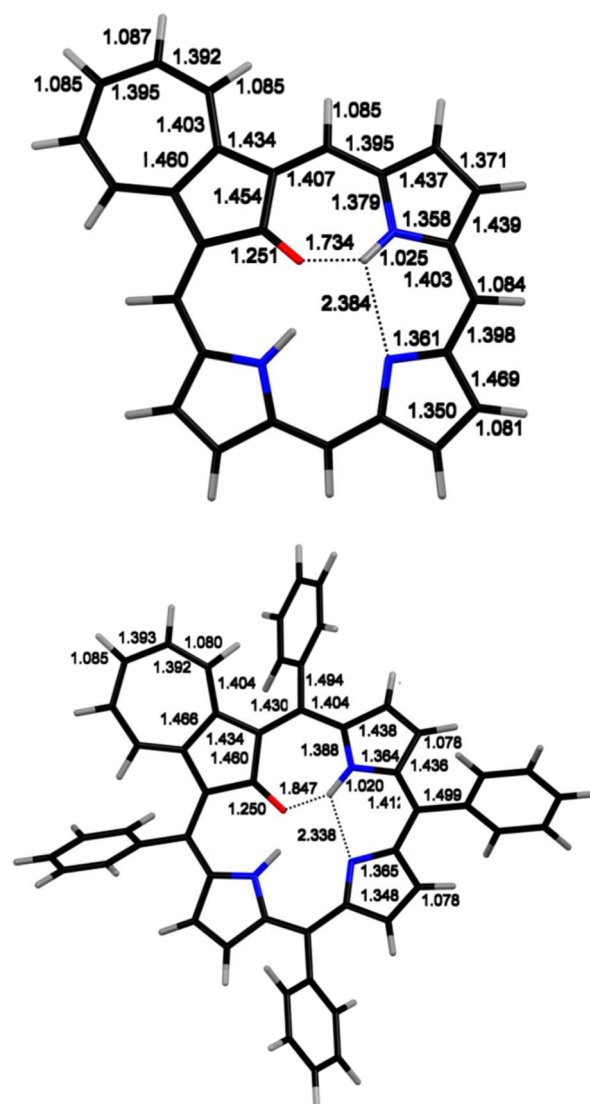
Figure 4. DFT-calculated bond lengths for **15** (upper) and **14a** (lower).

16A   16B

17A   17B
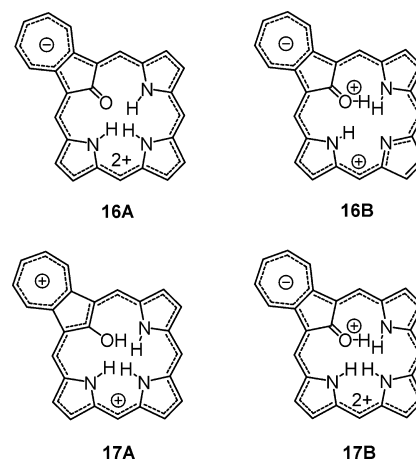
It is evident that the carbonyl unit is strongly influenced by π-bonding to the azuliporphyrin. In fact, all framework bond lengths were found by *Mogul* to be consistent with a generally delocalized π-system.[52] The *meso*-carbon atoms and the pyrrolic units form a generally planar motif as evidenced by the 0.186 Å

Table 3. Calculated Relative Energies (kcal/mol) and NICS Values (ppm) for Protonated Oxyazuliporphyrins

	$15H^+$	15^yH^+	15^xH^+	$15H_2^{2+}$
Rel. ΔG	0.00	23.40	16.71	****
B3LYP/**M06-2X**/B3LYP-D	0.00	23.98/**19.29**/24.04	16.88/**12.43**/17.00	****
NICS(0)/**NICS(1)zz**	-7.98/**-12.21**	-8.96/**-22.63**	-9.94/**-24.16**	-11.71/**-27.24**
NICS(a)/**NICS (1a)zz**	+6.70/**+17.38**	-7.43/**-8.29**	-8.74/**-10.27**	-2.22/**+0.95**
NICS(b)/**NICS(1b)zz**	-9.20/**-18.80**	-0.90/**-9.54**	-8.92/**-21.35**	-10.70/**-21.07**
NICS(c)/**NICS(1c)zz**	-6.89/**-18.03**	-9.11/**-16.94**	+0.33/**-3.02**	-11.35/**-39.01**
NICS(d)/**NICS(1d)zz**	-9.20/**-18.80**	-9.74/**-27.48**	-9.35/**-25.03**	-11.21/**-21.46**
NICS(e)/**NICS(1e)zz**	+14.36/**+28.04**	+2.19/**+4.97**	+2.20/**+4.84**	+0.26/**-6.41**

	$14H^+$	14^yH^+	14^xH^+	$14H_2^{2+}$
Rel. ΔG	0.00	10.70	7.80	****
B3LYP/**M06-2X**/B3LYP-D	0.00	11.14/**7.59**/11.83	8.72/**5.44**/9.18	****
NICS(0)/**NICS(1)zz**	-6.09/**-5.89**	-6.48/**-13.10**	-7.99/**-16.62**	-7.79/**-16.48**
NICS(a)/**NICS (1a)zz**	+11.11/**+24.35**	-11.59/**-15.30**	-12.18/**-16.14**	-9.11/**-12.56**
NICS(b)/**NICS(1b)zz**	-8.70/**-26.26**	-1.59/**-3.18**	-8.58/**-10.34**	-10.45/**-11.31**
NICS(c)/**NICS(1c)zz**	-6.31/**-9.16**	-8.41/**-27.88**	+0.20/**-9.53**	-9.78/**-36.41**
NICS(d)/**NICS(1d)zz**	-8.70/**-26.26**	-9.09/**-11.30**	-9.08/**-12.69**	-10.20/**-11.45**
NICS(e)/**NICS(1e)zz**	+16.74/**+34.93**	-2.86/**-6.97**	-2.49/**-6.64**	-2.88/**-8.92**

rms distance the framework atoms contained therein lie from the plane defined by the C21, N22, N23, and N24 core atoms. The 8.57(19)°, 6.66(19)°, and 8.08(17)° dihedral angles between the core and each of the three pyrrolic mean planes further quantify this observation. Remarkably, the dihedral angle between the oxyazulenyl plane and the core plane is 38.19(7)° with O25 lying 0.862(2) Å "above" and C2c lying 3.168(3) Å "below" the C21, N22, N23, and N24 core.

To quantify the accuracy of B3LYP/6-311++G** in predicting porphyrinoid geometry, a comparison between the calculated structure and the crystal structure of **14a** was performed (see Tables S2 and S3). Comparing representative bond lengths between the two structures revealed that both the XRD and calculated structures were in excellent agreement with the average bond length deviation being ~0.01 Å. However, the observed dihedral angles are slightly larger than had been predicted by the DFT calculations for **14a** in a vacuum, and these differences were attributed to crystal-packing forces. Experimental NMR data were collected in solution where the molecules can more freely take on a conformation that is lower

in energy than the solid-state/crystal structure, and this is likely to lead to the observed deviations.

The possibility of using oxyazuliporphyrins as macrocyclic ligands was investigated, and complexes of group 10 elements were targeted for study. It is worth noting that similar complexes of 21-hydroxy N-confused porphyrins[51] and 22-hydroxybenziporphyrins[53] have been reported previously. Tetraphenyloxyazuliporphyrin **14a** in chloroform was stirred with a saturated solution of nickel(II) acetate in methanol at room temperature, and following purification by column chromatography and recrystallization from chloroform−hexanes, the corresponding nickel(II) complex **18a** was isolated in 83% yield (Scheme 3). *tert*-Butyl oxyazuliporphyrin **14c** reacted similarly under these conditions to give the related metal complex **18b**. Palladium(II) acetate also reacted with **14a** or **14c** to give similar palladium(II) complexes **18c** and **18d**. In these reactions, the porphyrinoid and Pd(OAc)$_2$ were stirred at room temperature for 5−16 h, and the metalloporphyrinoids were isolated in excellent yields. The formation of the platinum(II) complex **18e** was more problematical. Heating
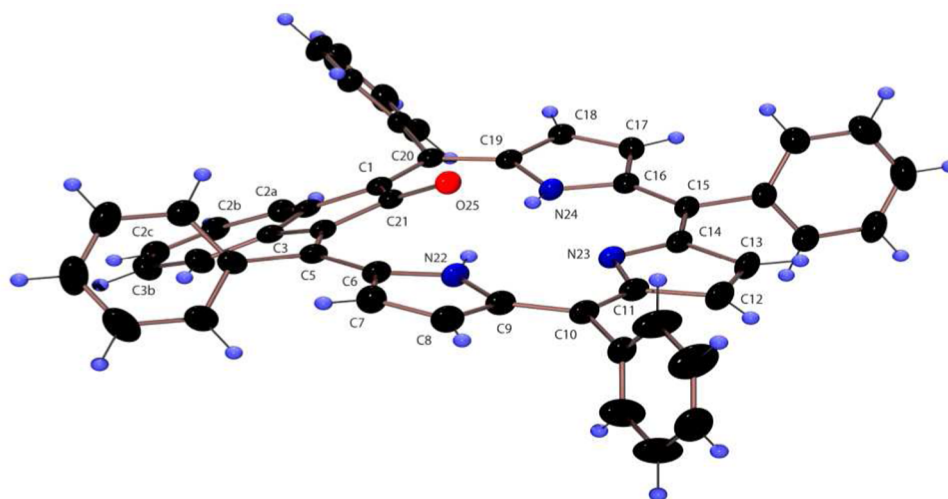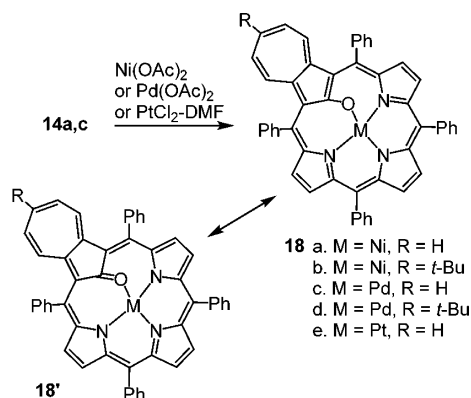
Figure 5. Color POV-Ray rendered ORTEP III drawing (50% probability level, hydrogen atoms rendered arbitrarily small for clarity) of oxyazuliporphyrin **14a**.

Scheme 3

samples of **14a** with platinum chloride gave unidentified green-colored materials. However, when the reaction was performed in dimethylformamide (DMF) at 150 °C, **18e** could be isolated in up to 45% yield.

The UV−vis spectra for these complexes showed that these complexes had lost the porphyrin-like appearance of the parent ligands (Figure 6). Nickel complex **18a** gave moderately strong absorptions at 378 and 499 nm, together with a weaker band at 626 nm. In addition, all of the metalloporphyrinoids gave a weak broad absorption between 800 and 900 nm. The *tert*-butyl complex **18b** gave a very similar UV−vis spectrum, but the major bands were bathochromically shifted by 3−4 nm. Palladium(II) complex **18c** gave absorptions at 384 and 517 nm and a weaker band at 619 nm, while the platinum complex produced absorptions at 391 and 511 nm, the former being somewhat stronger in this case, and weak absorptions at 618 and 648 nm. Overall, these results are remarkably similar, although the differences are sufficiently large to distinguish between the individual encapsulated metal cations. The proton NMR spectra for the complexes showed substantial downfield shifts to the protons on the seven-membered rings. For nickel complex **18a** in CDCl₃ (Figure 7), the azulene protons gave rise to three resonances at 6.37 (2H, d), 6.41 (1H, t), and 6.48 ppm (2H, t), while the pyrrolic protons appeared at 7.43 (2H, d), 7.61 (2H, s), and 8.06 ppm (2H, d). These results indicate that the macrocycle has a significant diamagnetic ring current,
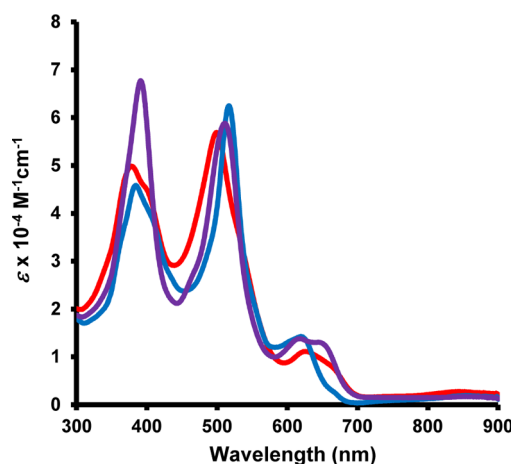

Figure 6. UV−vis spectra of metallo-oxyazuliporphyrins in chloroform: nickel(II) complex **18a** (red line), palladium(II) complex **18c** (blue line), and platinum(II) complex **18e** (purple line).
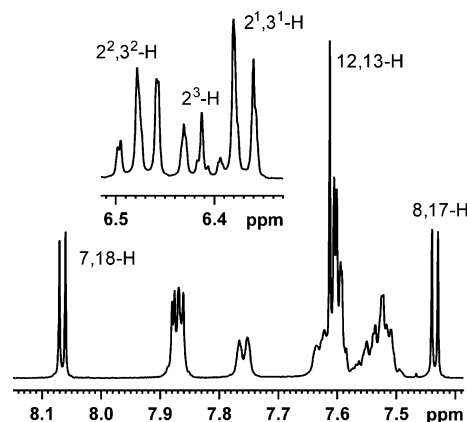

Figure 7. 500 MHz proton NMR spectrum of nickel complex **18a** in CDCl₃.

while the azulene protons fall into an intermediary region between the values expected for aromatic and olefinic protons. This may be caused by a disruption of the azulene conjugation pathway due to canonical forms such as **18′** (Scheme 3). For
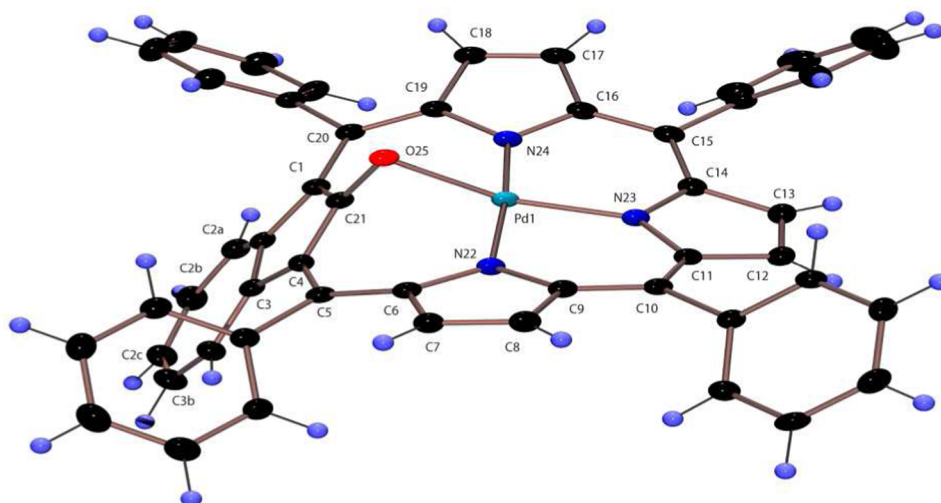
Figure 8. Color POV-Ray rendered ORTEP III drawings (50% probability level, hydrogen atoms rendered arbitrarily small for clarity) of palladium complex **18c**.
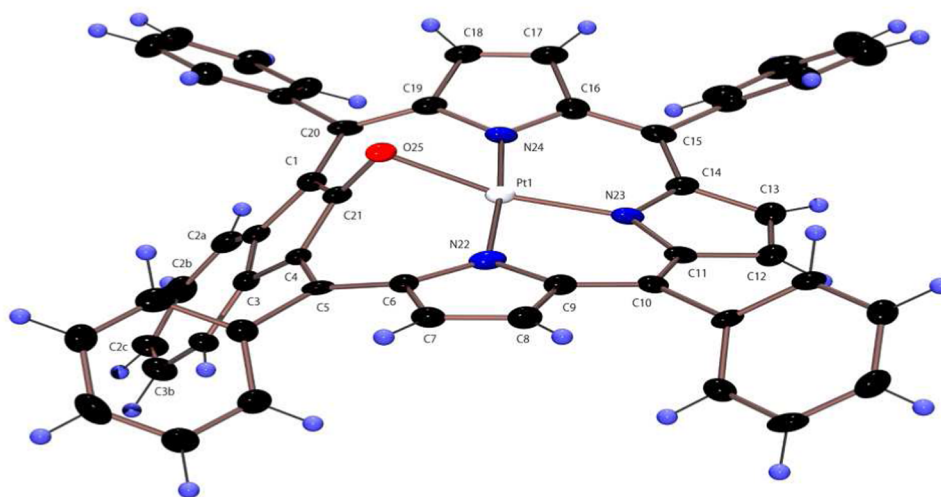

Figure 9. Color POV-Ray rendered ORTEP III drawings (50% probability level, hydrogen atoms rendered arbitrarily small for clarity) of platinum complex **18e**.

palladium complex **18c**, the azulene protons showed up between 6.10 and 6.29 ppm, while the pyrrolic protons appeared at 7.54 (2H, d), 7.62 (2H, s), and 8.15 ppm (2H, d). These results indicate that the diatropic ring current is a little larger for the palladium complex, while the azulene protons are shifted slightly upfield compared to **18a**. Platinum complex **18e** gave complicated second-order coupling for the azulene protons because the $2^1,3^1$ protons almost exactly coincide with the chemical shifts for the $2^2,2^3$ protons. For this reason, a 4H multiplet was observed at 6.19−6.24 ppm, and a 1H multiplet was seen at 6.30−6.35 ppm. Four of the pyrrolic protons were observed as two 2H doublets at 7.54 and 8.07 ppm, but the 12,13 protons were obscured by the phenyl resonances. In this case, the overall diatropicity and the chemical shifts for the azulene protons appear to lie between the results obtained for the nickel(II) and palladium(II) derivatives. The carbon-13 NMR spectra of **18a−e** confirm the presence of a plane of symmetry in these structures and the absence of carbonyl units. High-resolution mass spectra provided further support for these structures.

The structures of tetraphenyloxyazuliporphyrinato (TPOAP) complexes **18c** and **18e** were confirmed by single-crystal XRD analysis (Figures 8 and 9). These metalloporphyrinoids not only adopt remarkably similar conformations to one other but also strikingly resemble the structure previously reported for the copper(II) analogue.[30] This is clearly illustrated by the overlay of structures **13a**, **18c**, and **18e**, which was generated by a least-squares fit of the C21, N22, N23, and N24 core atoms (Figure 10). The nonazulene framework atoms are a little less planar than in the free-base, as evidenced by the 0.341 Å rms and 0.342 Å rms distances the respective atoms of **18c** and **18e** lie from the planes defined by their cores. In both compounds, the dihedral angles between the core and pyrrolic mean planes range between 6.7(1)° and 15.2(1)°. In **18c**, the dihedral angle between the oxyazulenyl plane and the core plane is 59.55(4)° with O25 lying 1.025(1) Å "above" and C2c lying 4.676(2) Å "below" the core. This is nearly indistinguishable from the 62.1° dihedral angle between the phenolate plane and three nitrogen (N3) plane reported for tetraphenyl-22-oxybenziporphyrinato-palladium(II), [(TPBPO)Pd^II].[53] Similarly, in **18e** the dihedral angle between the oxyazulenyl plane and the core plane is
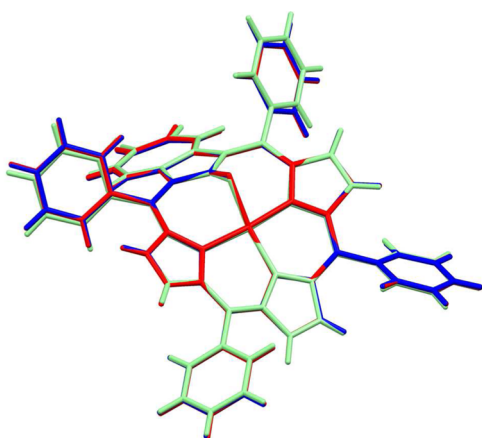
Figure 10. Mercury-rendered overlay of Pd(II) complex **18c** (blue), Pt(II) complex **18e** (red), and Cu(II) structure **13a** (green).

59.0(1)° with O25 lying 1.020(3) Å "above" and C2c lying 4.667(5) Å "below" the core. The previously reported copper analogue has a slightly smaller 57.05(8)° corresponding dihedral angle. These complexes may also be compared to the very recently reported six-coordinate ruthenium(II) complex, [(TPOAP)Ru^{II}(CO)(L)], L = *n*-butanol, which possesses a 48.0(4)° corresponding dihedral angle.[31]

The organic bond parameters of both metalated complexes were found by *Mogul* to be generally typical. Overall, the framework bond lengths appear to be consistent with overall delocalized bonding (Table 4).[54] In common with the 13 other monometalated azuliporphyrinoid structures that we and others have reported,[20−23,29−31,55,56] all of the C−C bond lengths of the azulene's cyclopentadienyl rings are rather distended to between 1.41 and 1.51 Å, suggesting that they all have significant single-bond character (Table 4). The C−O bond lengths for **18c**, **18e**, and **13a** (Table 4) were 1.308, 1.312, and 1.302 Å, respectively, and these values indicate that this unit retains substantial double bond character, reaffirming the significance of resonance contributors such as **18′** (Scheme 3). In both complexes, the M(II) ion is situated in a strained square planar coordination environment with the observed *trans*-N23−M−O25 bond angle being 162.03(6)° and 163.51(14)° for the respective Pd and Pt complexes (Table S1). This is similar to the corresponding 167.1(1)° angle observed for [(TPBPO)Pd^{II}],[53] 158.6(4)° angle observed for [(TPOAP)Ru^{II}(CO)(L)],[31] and the 157.22(8)° bond angle previously reported for copper(II) complex **13a**.[30] The conformations appear to be restricted as the M−C(21) separation is significantly shorter than the sum of van der Waals radii (1.4 Å for Cu, 1.63 Å for Pd, 1.72 Å for Pt, and 1.77 Å for C).[57] The Pd−C separation in **18c** is 2.457(2) Å compared to 2.571(2) Å in (TPBPO)Pd^{II}, and similar values are observed for the Ru, Pt, and Cu complexes with a Ru−C separation in [(TPOAP)Ru^{II}(CO)(L)] of 2.523(13) Å, a Pt−C separation of 2.443(5) Å in **18e**, and a Cu−C separation of 2.474(2) Å in **13a** (Table 1). These are all larger than those normally observed for M−C bond lengths and indicate that there are no significant carbon−metal bonding interactions. The three new structures for **14a**, **18c**, and **18e** add to a very limited number of porphyrinoids that possess an internal hydroxyl or carbonyl unit. In fact, of the over 750 000 structures in the Cambridge Structural Database, a CSD search returned only 14 metalated oxyporphyrinoids of this type, none

Table 4. Summary of Framework and Metal Coordination Sphere Bond Distances (Å) for Oxyazuliporphyrin 14a and Metal Complexes 13a, 18c, and 18e

	14a	18c (Pd)	18e (Pt)	13a (Cu)
M−C21		2.457(2)	2.443(5)	2.474(2)
M−O25		2.0178(15)	2.029(3)	1.9378(16)
M−N22		2.0002(17)	1.997(4)	1.990(2)
M−N23		1.9639(18)	1.962(4)	1.911(2)
M−N24		2.0057(17)	1.995(4)	2.003(2)
C21−O25	1.268(3)	1.308(2)	1.312(6)	1.302(3)
C2−C2a	1.419(4)	1.402(3)	1.409(7)	1.399(3)
C2a−C2b	1.383(4)	1.379(3)	1.352(7)	1.390(4)
C2b−C2c	1.380(4)	1.383(3)	1.383(8)	1.377(4)
C2c−C3b	1.382(4)	1.399(3)	1.399(7)	1.390(4)
C3b−C3a	1.408(4)	1.390(3)	1.380(7)	1.390(4)
C3a−C3	1.387(4)	1.401(3)	1.397(7)	1.397(3)
C21−C1	1.447(3)	1.423(3)	1.423(6)	1.425(3)
C1−C2	1.434(4)	1.435(3)	1.440(7)	1.432(3)
C2−C3	1.453(4)	1.468(3)	1.468(7)	1.465(3)
C3−C4	1.452(4)	1.434(3)	1.439(6)	1.437(3)
C4−C21	1.453(4)	1.422(3)	1.421(7)	1.432(3)
C4−C5	1.425(4)	1.426(3)	1.425(6)	1.426(3)
C5−C6	1.407(4)	1.403(3)	1.390(7)	1.398(3)
C6−N22	1.378(4)	1.399(3)	1.408(6)	1.406(3)
C6−C7	1.433(4)	1.437(3)	1.432(6)	1.444(3)
C7−C8	1.366(4)	1.349(3)	1.354(7)	1.348(3)
C8−C9	1.416(4)	1.438(3)	1.437(7)	1.439(3)
C9−N22	1.373(3)	1.362(3)	1.364(6)	1.373(3)
C9−C10	1.411(4)	1.416(3)	1.408(7)	1.416(3)
C10−C11	1.391(4)	1.393(3)	1.395(7)	1.390(3)
C11−N23	1.377(3)	1.378(3)	1.378(6)	1.387(3)
C11−C12	1.452(4)	1.456(3)	1.461(7)	1.444(3)
C12−C13	1.333(4)	1.352(3)	1.339(7)	1.345(4)
C13−C14	1.468(4)	1.449(3)	1.455(7)	1.447(3)
C14−N23	1.367(4)	1.374(3)	1.382(6)	1.370(3)
C14−C15	1.402(4)	1.399(3)	1.398(7)	1.395(3)
C15−C16	1.421(4)	1.419(3)	1.428(7)	1.421(3)
C16−N24	1.357(3)	1.361(3)	1.349(7)	1.370(3)
C16−C17	1.427(4)	1.452(3)	1.452(7)	1.445(4)
C17−C18	1.364(4)	1.346(3)	1.346(7)	1.347(4)
C18−C19	1.427(4)	1.448(3)	1.453(7)	1.442(3)
C19−N24	1.392(3)	1.404(3)	1.409(6)	1.414(3)
C19−C20	1.400(4)	1.395(3)	1.390(7)	1.390(3)
C20−C1	1.424(4)	1.404(3)	1.433(7)	1.428(3)

of which contained platinum,[58] and only two different solvates of the aforementioned (TPBPO)Pd^{II} complex were coordinated to palladium.[53]

■ CONCLUSIONS

An improved synthesis of 21-oxyazuliporphyrins has been developed that involves reacting tetraarylazuliporphyrins with silver(I) acetate in refluxing chloroform−acetonitrile. The characteristics of this unusual porphyrinoid system have been

probed using spectroscopic methods, DFT calculations, and single-crystal X-ray diffraction. These techniques all indicate that the keto-tautomer is favored rather than a hydroxyazuliporphyrin structure. Although this system formally possesses a 24π electron delocalization pathway, proton NMR spectroscopy and NICS calculations both indicate that the macrocycle is moderately diatropic. The NICS results suggest that the seven-membered ring may have antiaromatic character, although the proton NMR spectra indicate that the azulene protons are nonaromatic rather than paratropic. Oxyazuliporphyrins appear to be good ligands for late transition metal cations, and stable complexes of Ni(II), Pd(II), and Pt(II) have been prepared. These results indicate that the azuliporphyrin framework has great potential for metal cation binding, and importantly, the properties of this system differ significantly from any other known porphyrinoid ligand.

■ EXPERIMENTAL SECTION

Melting points are uncorrected. NMR spectra were recorded using a 400 or 500 MHz NMR spectrometer and were run at 300 K unless otherwise indicated. ^{1}H NMR values are reported as chemical shifts δ, relative integral, multiplicity (s, singlet; d, doublet; t, triplet; q, quartet; m, multiplet; br, broad peak) and coupling constant (J). Chemical shifts are reported in parts per million (ppm) relative to CDCl$_3$ (^{1}H residual CHCl$_3$ δ 7.26, ^{13}C CDCl$_3$ triplet δ 77.23) or d_5-pyridine (upfield residual d_4-pyridine resonance δ 7.19 ppm, ^{13}C upfield C$_6$D$_4$HN triplet δ 123.5 ppm), and coupling constants were taken directly from the spectra. NMR assignments were made with the aid of ^{1}H–^{1}H COSY, HSQC, DEPT-135, and NOE difference proton NMR spectroscopy. Two-dimensional experiments were performed using standard software. HRMS was performed using a double focusing magnetic sector instrument. ^{1}H and ^{13}C NMR spectra for all new compounds are reported in Supporting Information.

Copper(II) Complex of 5,10,15,20-Tetrakis(4-chlorophenyl)-21-oxyazuliporphyrin (9b). Copper(II) acetate monohydrate (158 mg, 0.79 mmol) was added to a solution of **8b** (60.3 mg, 0.0599 mmol) in pyridine (120 mL), and the resulting mixture was stirred under an atmosphere of nitrogen for 5 min. The mixture was diluted with chloroform (60 mL), washed with water (150 mL) and dried over sodium sulfate. The solvents were removed under reduced pressure, and the residue was purified by column chromatography on grade 3 alumina, eluting with 20% hexanes−dichloromethane. The product was collected as a red fraction. Recrystallization from chloroform−hexanes gave **10b** (10.5 mg, 0.0118 mmol, 16%) as shiny dark-green crystals, mp > 300 °C; UV−vis (pyridine): λ_{max} (log ε) 368 (4.56), 418 (4.58), 522 (4.77), 627 (3.93), 670 nm (sh, 3.70); HRMS electrospray ionization (EI) calcd for C$_{50}$H$_{27}$Cl$_4$CuN$_3$O 888.0204, found 888.0204.

5,10,15,20-Tetrakis(4-chlorophenyl)-21-oxyazuliporphyrin (14b). Method A. Copper complex **13b** (34.5 mg, 0.0387 mmol) was stirred with 10% TFA−chloroform (35 mL) for 15 min at room temperature. The mixture was washed with water and 5% sodium bicarbonate solution, dried over sodium sulfate, and evaporated to dryness. The residue was purified by column chromatography on grade 3 alumina, eluting with 50% dichloromethane−chloroform. The demetalated product eluted as a purple band. Recrystallization from chloroform−hexanes afforded **14b** (22.2 mg, 0.0268 mmol, 69%) as shiny green crystals, mp 349−350 °C dec. Method B. A mixture of azuliporphyrin **7b** (50.0 mg, 0.0615 mmol) and silver(I) acetate (20.4 mg) in chloroform (30 mL) and acetonitrile (30 mL) was stirred under reflux for 16 h. The mixture was cooled to room temperature and then evaporated under reduced pressure. The residue was purified by column chromatography on grade 2 basic alumina, eluting initially with 80% hexanes−dichloromethane, then dichloromethane, and finally with 4% ethyl acetate−dichloromethane. The main reddish purple fraction corresponded to the product. The upper portion of the column was removed and stored at room temperature overnight. This was treated with chloroform and filtered, and the solution was evaporated to dryness. The residue was chromatographed as noted

above and gave an additional product fraction. The combined fractions were recrystallized from chloroform−methanol to give **14b** (33.2 mg, 0.40 mmol, 65%) as dark green crystals, mp > 300 °C; UV−vis (1% Et$_3$N−CH$_2$Cl$_2$): λ_{max} (log ε) 363 (4.70), 407 (4.64), 449 (sh, 4.59), 473 (sh, 4.65), 522 (5.09), 597 (sh, 4.12), 645 (4.01), 714 nm (3.78); UV−vis (1% TFA−CH$_2$Cl$_2$): λ_{max} (log ε) 422 (sh, 4.63), 465 (sh, 4.72), 523 (4.98), 619 (3.94), 683 (3.80), 855 nm (4.14); ^{1}H NMR (500 MHz, CDCl$_3$): δ 5.23 (2H, d, J = 10.6 Hz, 2^1,3^1-H), 5.47 (1H, t, J = 9.4 Hz, 2^3-H), 5.81 (2H, t, J = 10.1 Hz, 2^2,3^2-H), 6.34 (2H, br, 2 × NH), 7.37 (2H, d, J = 4.9 Hz, 8,17-H), 7.51 (2H, s, 12,13-H), 7.53 (4H, d, J = 8.3 Hz, 10,15-m-Ph), 7.62 (4H, d, J = 8.3 Hz, 5,20-m-Ph), 7.67 (4H, d, J = 8.3 Hz, 10,15-o-Ph), 7.80 (2H, d, J = 4.9 Hz, 7,18-H), 7.87 (4H, d, J = 8.3 Hz, 5,20-o-Ph); ^{13}C NMR (125 MHz, CDCl$_3$): δ 116.9, 125.8, 126.5 (8,17-CH), 127.7 (10,15-m-Ph), 128.0 (5,20-m-Ph), 129.3 (7,18-CH), 130.4, 131.1 (2^1,3^1-CH), 132.0 (2^3-CH), 134.0, 134.6 (10,15-o-Ph), 135.1 (12,13-CH), 135.2, 135.5 (5,20-o-Ph), 138.5, 139.7, 140.0 (2^2,3^2-CH), 141.0, 144.6, 147.4, 150.8, 162.6 (C═O); ^{1}H NMR (500 MHz, TFA−CDCl$_3$): δ 7.34−7.44 (5H, m), 7.80−7.84 (6H, m), 7.90−7.96 (4H, br m), 8.00 (4H, d, J = 8.3 Hz), 8.24−8.31 (8H, m); ^{13}C NMR (125 MHz, TFA−CDCl$_3$): δ 116.3, 120.4, 127.4, 129.3, 130.2, 132.1, 132.2, 134.0, 136.2 (br), 136.8, 137.0, 137.5, 138.1, 138.9, 139.9, 140.0, 141.1, 142.3, 146.9, 150.3; HRMS (FAB) calcd for C$_{50}$H$_{29}$Cl$_4$N$_3$O + H 828.1143, found 828.1140. Anal. Calcd for C$_{50}$H$_{29}$Cl$_4$N$_3$O.H$_2$O: C, 70.85; H, 3.69; N, 4.96. Found: C, 70.35; H, 3.70; N, 4.91%.

5,10,15,20-Tetraphenyl-21-oxyazuliporphyrin (14a). Tetraphenylazuliporphyrin **7a** (41.4 mg, 0.0613 mmol) was reacted with silver(I) acetate (20.4 mg) using method B to give the oxyazuliporphyrin (22.9 mg, 0.0331 mmol, 54%) as dark green crystals, mp > 300 °C (chloroform−methanol; lit. mp 321−322 °C dec); UV−vis (1% Et$_3$N−CH$_2$Cl$_2$): λ_{max} (log ε) 361 (4.67), 406 (4.61), 449 (sh, 4.54), 520 (5.10), 601 (4.04), 644 (3.93), 715 nm (3.65); UV−vis (1% TFA−CH$_2$Cl$_2$): λ_{max} (log ε) 344 (4.37), 417 (sh, 4.63), 462 (sh, 4.72), 519 (5.01), 614 (3.98), 674 (3.77), 848 nm (4.18); ^{1}H NMR (500 MHz, CDCl$_3$): δ 5.16 (2H, d, J = 10.6 Hz, 2^1,3^1-H), 5.37 (1H, t, J = 9.4 Hz, 2^3-H), 5.68 (2H, t, J = 10.1 Hz, 2^2,3^2-H), 6.47 (2H, br, 2 × NH), 7.38 (2H, d, J = 4.9 Hz, 8,17-H), 7.52 (2H, s, 12,13-H), 7.53−7.56 (6H, m, 10,15-m,p-Ph), 7.58−7.63 (6H, m, 5,20-m,p-Ph), 7.75−7.78 (4H, m, 10,15-o-Ph), 7.84 (2H, d, J = 4.9 Hz, 7,18-H), 7.93−7.95 (4H, m, 5,20-o-Ph); ^{13}C NMR (125 MHz, CDCl$_3$): δ 118.0, 125.9, 126.5 (8,17-CH), 127.4 (10,15-m-Ph), 127.55, 127.6 (5,20-m-Ph), 128.4 (5,20-p-Ph), 129.4 (7,18-CH), 131.0 (2^1,3^1-CH), 131.4 (2^3-CH), 131.7, 133.5 (10,15-o-Ph), 134.6 (5,20-o-Ph), 135.1 (12,13-CH), 139.4 (2^2,3^2-CH), 140.3, 141.2, 141.5, 144.8, 147.8, 150.6, 162.7 (C═O); ^{1}H NMR (500 MHz, TFA−CDCl$_3$): δ 7.25−7.30 (5H, m), 7.79−7.82 (8H, m), 7.90−7.95 (6H, m), 8.06−8.09 (4H, m), 8.23 (2H, d, J = 1.5 Hz), 8.29 (2H, d, J = 4.9 Hz), 8.32−8.38 (4H, br m); ^{13}C NMR (125 MHz, TFA−CDCl$_3$): δ 117.0, 120.5, 127.2, 128.7, 129.5, 130.1, 130.4 (br), 132.0, 132.3, 135.1, 135.9 (br), 137.1 (br), 137.9, 138.0, 138.6, 139.2, 140.2, 142.2, 146.8, 150.4; HRMS (FAB) calcd for C$_{50}$H$_{33}$N$_3$O + H 692.2702, found 692.2701.

5,10,15,20-Tetraphenyl-2^3-*tert*-butyl-21-oxyazuliporphyrin (14c). Using the previous procedure, *tert*-butylazuliporphyrin **7c** (67.2 mg, 0.0919 mmol) was reacted with silver(I) acetate (10.2 mg) in 45 mL of chloroform and 45 mL of acetonitrile to give the oxyazuliporphyrin (37.0 mg, 0.0495 mmol, 54%) as dark crystals, mp > 300 °C dec (chloroform−methanol); UV−vis (1% Et$_3$N−CH$_2$Cl$_2$): λ_{max} (log ε) 362 (4.65), 405 (4.60), 445 (sh, 4.53), 471 (sh, 4.58), 525 (5.12), 599 (sh, 4.05), 643 (3.91), 715 nm (3.77); UV−vis (5% TFA−CH$_2$Cl$_2$): λ_{max} (log ε) 348 (4.44), 401 (sh, 4.56), 460 (sh, 4.74), 518 (5.04), 609 (4.06), 669 (3.84), 839 nm (4.20); ^{1}H NMR (500 MHz, CDCl$_3$): δ 0.92 (9H, s, t-Bu), 5.17 (2H, d, J = 11.6 Hz, 2^1,3^1-H), 5.87 (2H, d, J = 11.6 Hz, 2^2,3^2-H), 6.71 (2H, br, 2 × NH), 7.34 (2H, d, J = 4.9 Hz, 8,17-H), 7.49 (2H, s, 12,13-H), 7.52−7.55 (6H, m, 10,15-m,p-Ph), 7.59−7.63 (6H, m, 5,20-m,p-Ph), 7.74−7.77 (4H, m, 10,15-o-Ph), 7.78 (2H, d, J = 4.9 Hz, 7,18-H), 7.91−7.94 (4H, m, 5,20-o-Ph); ^{13}C NMR (125 MHz, CDCl$_3$): δ 30.3 (C(CH$_3$)$_3$), 36.3 (C(CH$_3$)$_3$), 117.9, 125.7, 126.2 (8,17-CH), 127.3 (10,15-m-Ph), 127.47, 127.51 (5,20-m-Ph), 128.4 (5,20-p-Ph), 129.2 (7,18-CH), 130.8 (2^1,3^1-CH), 131.5, 133.5 (10,15-o-Ph), 134.5 (5,20-o-Ph), 134.9

(12,13-CH), 137.7 (2^2,3^2-CH), 140.5, 141.1, 141.6, 144.4, 148.7, 149.9, 154.5, 162.7 (C=O); ^{1}H NMR (500 MHz, TFA–CDCl$_3$): δ 1.22 (9H, s), 7.25 (2H, d, J = 11.3 Hz), 7.44 (2H, d, J = 11.3 Hz), 7.79–7.82 (8H, m), 7.90–7.96 (6H, br m), 8.08–8.11 (4H, m), 8.26–8.27 (2H, d, J = 1.3 Hz), 8.28 (2H, d, J = 4.9 Hz), 8.33–8.44 (4H, br m); ^{13}C NMR (125 MHz, TFA–CDCl$_3$): δ 31.1, 38.9, 116.9, 120.6, 126.9, 128.6, 129.4, 129.9, 130.4 (br), 131.79, 131.84, 131.86, 134.8, 135.9 (br), 137.1, 137.8, 138.0, 138.2, 139.0, 142.0, 146.4, 149.8; HRMS (EI) calcd for C$_{54}$H$_{41}$N$_3$O 747.3249, found 747.3248. Anal. Calcd for C$_{54}$H$_{41}$N$_3$O.H$_2$O.CHCl$_3$: C, 74.62; H, 5.01; N, 4.75. Found: C, 74.85; H, 5.02; N, 4.81%.

2^3,5,10,15,20-Pentaphenyl-21-oxazuliporphyrin (14d). Pentaphenylazuliporphyrin **7d** (23.0 mg, 0.0306 mmol) reacted with silver acetate (10.2 mg, mmol) under the foregoing conditions to give **14d** (15.2 mg, 0.0198 mmol, 65%) as dark crystals, mp > 300 °C dec (chloroform−methanol); UV−vis (CH$_2$Cl$_2$): λ_{max} (log ε) 368 (4.77), 410 (4.73), 452 (sh, 4.58), 533 (5.24), 609 (sh, 4.20), 651 (sh, 3.96), 730 nm (4.03); UV−vis (1% TFA−CH$_2$Cl$_2$): λ_{max} (log ε) 370 (4.63), 405 (sh, 4.61), 453 (sh, 4.71), 524 (5.05), 613 (4.13), 673 (3.86), 849 nm (4.24); ^{1}H NMR (500 MHz, CDCl$_3$): δ 5.21 (2H, d, J = 11.5 Hz, 2^1,3^1-H), 5.95 (2H, t, J = 11.5 Hz, 2^2,3^2-H), 6.62 (2H, br, 2 × NH), 7.08–7.11 (2H, m, 2^3-o-Ph), 7.20–7.23 (3H, m, 2^3-m,p-Ph), 7.36 (2H, d, J = 4.9 Hz, 8,17-H), 7.51 (2H, s, 12,13-H), 7.53–7.56 (6H, m, 10,15-m,p-Ph), 7.58–7.64 (6H, m, 5,20-m,p-Ph), 7.75–7.78 (4H, m, 10,15-o-Ph), 7.83 (2H, d, J = 4.9 Hz, 7,18-H), 7.94–7.97 (4H, m, 5,20-o-Ph); ^{13}C NMR (125 MHz, CDCl$_3$): δ 118.1, 125.8 (2^3-o-Ph), 125.9, 126.5 (8,17-CH), 127.4 (10,15-m-Ph), 127.56, 127.58 (5,20-m-Ph), 128.1 (5,20-p-Ph), 128.5 (2^3-m-Ph), 128.6, 129.4 (7,18-CH), 130.7 (2^1,3^1-CH), 131.7, 133.5 (10,15-o-Ph), 134.6 (5,20-o-Ph), 135.1 (12,13-CH), 139.5 (2^2,3^2-CH), 140.4, 141.2, 141.5, 141.9, 144.2, 144.8, 148.4, 149.6, 162.7 (C=O); ^{1}H NMR (500 MHz, TFA-CDCl$_3$): δ 7.44 (2H, d, J = 11.2 Hz), 7.53 (5H, m), 7.64 (2H, d, J = 11.2 Hz), 7.95–7.98 (8H, m), 8.07–8.11 (6H, m), 8.24–8.27 (4H, m), 8.40 (2H, s), 8.45 (2H, d, J = 4.8 Hz), 8.50–8.58 (4H, br m); ^{13}C NMR (125 MHz, TFA–CDCl$_3$): δ 117.0, 120.9, 127.0, 128.1, 128.6, 129.3, 129.5, 129.97, 130.01, 131.9, 132.0, 135.0, 135.9 (br), 136.7, 137.9, 138.2, 138.9, 139.2, 141.1, 142.1, 146.7, 150.2, 154.4 (br); HRMS (EI) calcd for C$_{56}$H$_{37}$N$_3$O 767.2937, found 767.2942. Anal. Calcd for C$_{56}$H$_{37}$N$_3$O.0.6CHCl$_3$: C, 80.97; H, 4.51; N, 5.01. Found: C, 80.58; H, 4.37; N, 5.01%.

Nickel(II) Complex of 5,10,15,20-Tetraphenyl-21-oxyazuliporphyrin (18a). A saturated solution of nickel(II) acetate in methanol (25 mL) was added to a solution of oxyazuliporphyrin **14a** (23.3 mg, 0.0345 mmol) in chloroform (25 mL), and the mixture was stirred at room temperature for 15 min. The mixture was diluted with chloroform and washed with water (×2), and the organic solution was evaporated under reduced pressure. The residue was purified by column chromatography on grade 3 alumina, eluting with 20% hexanes−dichloromethane, and the product eluted as a reddish-brown fraction. Evaporation of the solvent and recrystallization of the resulting residue from chloroform−hexanes gave the nickel complex (21.5 mg, 0.0287 mmol, 83%) as dark crystals, mp > 350 °C dec; UV−vis (CHCl$_3$): λ_{max} (log ε) 378 (4.70), 399 (sh, 4.65), 499 (4.75), 626 (4.05), 843 nm (3.44); ^{1}H NMR (500 MHz, CDCl$_3$): δ 6.37 (2H, d, J = 10.1 Hz, 2^1,3^1-H), 6.40–6.43 (1H, m, 2^3-H), 6.46–6.50 (2H, m, 2^2,3^2-H), 7.43 (2H, d, J = 5.1 Hz, 8,17-H), 7.49–7.57 (6H, m), 7.59–7.64 (10H, m), 7.76 (2H, d, J = 6.8 Hz), 7.85–7.89 (4H, m), 8.06 (2H, d, J = 4.9 Hz, 7,18-H); ^{13}C NMR (125 MHz, CDCl$_3$): δ 115.3, 119.6, 126.4 (8,17-CH), 127.5, 127.6, 128.4, 131.3 (2^1,3^1-CH), 132.1 (2^3-CH), 133.0, 133.4, 133.9, 134.9, 135.1, 136.1 (2^2,3^2-CH), 138.4 (7,18-CH), 138.6, 140.3, 141.6, 142.7, 152.3, 153.2, 156.3; HRMS (EI) calcd for C$_{50}$H$_{31}$N$_3$NiO 747.1820, found 747.1810. Anal. Calcd for C$_{50}$H$_{31}$N$_3$NiO.CHCl$_3$: C, 70.58; H, 3.72; N, 4.84. Found: C, 70.35; H, 3.70; N, 4.85%.

Nickel(II) Complex of 5,10,15,20-Tetraphenyl-2^3-$tert$-butyl-21-oxyazuliporphyrin (18b). **14c** (15.0 mg, 0.020 mmol) in chloroform (16 mL) was reacted with a saturated solution of nickel(II) acetate in methanol (16 mL) for 1 h under the foregoing conditions. Recrystallization from chloroform−hexanes gave the metal complex (13.4 mg, 0.0167 mmol, 83%), mp > 300 °C; UV−vis

(CHCl$_3$): λ_{max} (log ε) 381 (4.70), 400 (sh, 4.66), 503 (4.78), 624 (4.08), 848 nm (3.38); ^{1}H NMR (500 MHz, CDCl$_3$): δ 1.11 (9H, s, t-Bu), 6.35 (2H, d, J = 11.4 Hz, 2^1,3^1-H), 6.65 (2H, d, J = 11.4 Hz, 2^2,3^2-H), 7.45 (2H, d, J = 5.1 Hz, 8,17-H), 7.49–7.57 (6H, m), 7.59–7.65 (8H, m), 7.63 (2H, s, 12,13-H), 7.77 (2H, br d, J = 7.1 Hz), 7.87–7.90 (4H, m), 8.05 (2H, d, J = 5.1 Hz, 7,18-H); ^{13}C NMR (125 MHz, CDCl$_3$): δ 31.1 (C(CH$_3$)$_3$), 37.5 (C(CH$_3$)$_3$), 115.1, 119.6, 126.1 (8,17-CH), 127.5, 128.4, 131.0 (2^1,3^1-CH), 133.1, 133.4, 133.7 (12,13-CH), 134.5 (2^2,3^2-CH), 134.8. 135.1, 138.2 (7,18-CH), 138.6, 140.5, 141.72, 141.76, 152.0, 153.0, 155.7, 156.0; HRMS (EI) calcd for C$_{54}$H$_{39}$N$_3$NiO 803.2447, found 803.2482.

Palladium(II) Complex of 5,10,15,20-Tetraphenyl-21-oxyazuliporphyrin (18c). A mixture of **10a** (29.3 mg, 0.0424 mmol) and palladium(II) acetate (21.0 mg, 0.93 mmol) in chloroform (30 mL) and methanol (30 mL) was stirred at room temperature for 5 h. The mixture was washed with water and dried over sodium sulfate, and the solvent was evaporated under reduced pressure. The residue was run through a grade 3 alumina column, eluting with 20% hexanes−dichloromethane, and the product was collected as a pinkish-brown fraction. Following evaporation of the solvent, the residue was recrystallized from chloroform−hexanes to give the palladium(II) complex (24.7 mg, 0.031 mmol, 73%) as dark crystals, mp 322−324 °C dec; UV−vis (CHCl$_3$): λ_{max} (log ε) 384 (4.66), 407 (sh, 4.59), 517 (4.79), 619 (4.15), 666 (sh, 3.42), 854 nm (3.30); ^{1}H NMR (500 MHz, CDCl$_3$): δ 6.10 (2H, d, J = 10.2 Hz, 2^1,3^1-H), 6.21 (1H, t, J = 9.3 Hz, 2^3-H), 6.29 (2H, t, J = 9.9 Hz, 2^2,3^2-H), 7.54 (2H, d, J = 5.1 Hz, 8,17-H), 7.54–7.57 (6H, m), 7.61–7.66 (8H, m), 7.70–7.73 (2H, m), 7.76–7.79 (2H, m), 7.98–8.01 (4H, m), 8.15 (2H, d, J = 5.1 Hz, 7,18-H); ^{13}C NMR (125 MHz, CDCl$_3$): δ 115.9, 117.4, 125.5, 127.27, 127.33, 127.37, 127.4, 128.4, 131.0, 131.5, 132.5, 132.9, 133.1, 133.2, 135.3, 136.0, 136.95, 136.98, 140.3, 140.4, 141.4, 149.8, 150.6, 153.0; HRMS (FAB) calcd for C$_{50}$H$_{31}$N$_3$OPd 795.1502, found 795.1504. Anal. Calcd for C$_{50}$H$_{29}$Cl$_4$N$_3$O.^{1}/$_3$CHCl$_3$: C, 72.31; H, 3.78; N, 5.02. Found: C, 72.12; H, 3.76; N, 4.80%.

Palladium(II) Complex of 5,10,15,20-Tetraphenyl-2^3-$tert$-butyl-21-oxyazuliporphyrin (18d). **14c** (15.0 mg, 0.0201 mmol) was reacted with palladium acetate (10.5 mg, 0.047 mmol) in chloroform (15 mL) and methanol (15 mL) for 16 h using the procedure described above. Recrystallization from chloroform−methanol gave the complex (15.5 mg, 0.0182 mmol, 91%) as dark crystals, mp > 300 °C; UV−vis (CHCl$_3$): λ_{max} (log ε) 386 (4.66), 521 (4.85), 620 (4.19), 666 (sh, 3.47), 856 nm (3.31); ^{1}H NMR (500 MHz, d_5-pyridine): δ 0.85 (9H, s, t-Bu), 6.45 (2H, d, J = 11.2 Hz, 2^1,3^1-H), 6.82 (2H, d, J = 11.2 Hz, 2^2,3^2-H), 7.58–7.66 (12H, m), 7.71 (2H, d, J = 5.1 Hz, 8,17-H), 7.83–7.86 (4H, m), 7.93 (2H, d, J = 7.4 Hz), 8.06 (4H, d, J = 7.3 Hz), 8.28 (2H, d, J = 5.1 Hz, 7,18-H); ^{13}C NMR (125 MHz, d_5-pyridine): δ 30.4, 37.1, 116.6, 117.9, 125.9, 127.9, 127.99, 128.02, 129.1, 131.4, 133.4, 133.5, 133.7, 134.4, 135.1, 137.1, 137.8, 140.2, 140.7, 141.7, 151.0, 152.9; HRMS (EI) calcd for C$_{54}$H$_{39}$N$_3$OPd + H 852.2206, found 852.2235.

Platinum(II) Complex of 5,10,15,20-Tetraphenyl-21-oxyazuliporphyrin (18e). A mixture of oxyazuliporphyrin **14a** (30.5 mg, 0.0452 mmol) and platinum(II) chloride (24.3 mg, 0.091 mmol) in DMF were heated with an oil bath set to ~150 °C for 90 min. The solution was cooled, diluted with chloroform, and washed with water. The solvent was removed on a rotary evaporator, initially using a water aspirator and then an oil pump, to remove residual DMF. The residue was purified on a grade 3 alumina column, eluting with 20% hexanes−dichloromethane. Initially, an unidentified green band eluted followed by a greyish-pink band corresponding to the product. The solvent was evaporated, and the residue recrystallized from chloroform−hexanes to give the platinum complex (18.0 mg, 0.0204 mmol, 45%) as dark green crystals, mp 329−330 °C dec; UV−vis (CHCl$_3$): λ_{max} (log ε) 391 (4.83), 511 (4.76), 618 (4.14), 648 nm (4.11); ^{1}H NMR (500 MHz, CDCl$_3$): δ 6.19–6.24 (4H, m, 2^1,2^2,3^1,3^2-H), 6.30–6.35 (1H, m, 2^3-H), 7.54 (2H, d, J = 5.2 Hz, 8,17-H), 7.54–7.57 (6H, m), 7.60–7.65 (8H, m), 7.70–7.73 (2H, m), 7.77–7.80 (2H, m), 7.96 (4H, br d, J = 6.5 Hz), 8.07 (2H, d, J = 5.2 Hz, 7,18-H); ^{13}C NMR (125 MHz, CDCl$_3$): δ 115.1, 116.5, 124.5, 127.2, 127.52, 127.58, 127.60, 127.7, 128.8, 129.9, 130.1, 132.97, 133.02, 133.2, 135.6, 137.1, 137.6, 138.3,

140.2, 141.0, 143.3, 148.2, 148.5, 151.5; HRMS (FAB) calcd for $C_{50}H_{31}N_3OPt$ 884.2115, found 884.2115.

Computational Studies. All calculations in this study were performed using the Gaussian 09 suite of programs.[59] The geometries of the porphyrinoid systems were optimized using B3LYP with a 6-311++G** basis set. The resulting Cartesian coordinates can be found in the Supporting Information. Frequency calculations at the same level of theory were used and confirmed all the stationary points were minima. In addition, electronic single-point energies were calculated using M06-2X and B3LYP-D functionals, in both cases with a 6-311+ +G** basis set. Gaussview running on an OS X platform was used to visualize the 3D conformations of the optimized structures. Two types of NMR calculations were used in this study. The first involved using the GIAO method[60] to obtain NICS values, and the second calculated using CGST to obtain AICD plots.[44] NICS(0) was calculated at the mean position of all the heavy atoms that make up the porphyrinoid core. NICS(a), NICS(b), NICS(c), NICS(d), and NICS(e) values were obtained by applying the same method to the mean position of the heavy atoms that comprise the individual rings of each macrocycle. In addition, NICS(1)$_{zz}$, NICS(1a)$_{zz}$, NICS(1b)$_{zz}$, NICS(1c)$_{zz}$, NICS-(1d)$_{zz}$, and NICS(1e)$_{zz}$ were obtained by applying the same method to ghost atoms placed 1 Å above each of the corresponding NICS(0) points and extracting the zz contribution of the magnetic tensor.[48,61] AICD plots for all the compounds were plotted using Gaussview at different isosurface values and can be found in the Supporting Information.

■ ASSOCIATED CONTENT

Ⓢ Supporting Information

The Supporting Information is available free of charge on the ACS Publications website at DOI: 10.1021/acs.inorg-chem.5b01587.

> X-ray crystallographic information for **14a**. (CIF)
> X-ray crystallographic information for **18c**. (CIF)
> X-ray crystallographic information for **18e**. (CIF)
> Experimental details for the X-ray crystallography. (PDF)
> Selected UV–vis, ^{1}H NMR, ^{1}H–^{1}H COSY, HSQC, DEPT-135, ^{13}C NMR, and mass spectra. (PDF)
> Tables and figures giving Cartesian coordinates and AICD plots. (PDF)

■ AUTHOR INFORMATION

Corresponding Author
*E-mail: tdlash@ilstu.edu.

Notes
The authors declare no competing financial interest.

■ ACKNOWLEDGMENTS

■ REFERENCES

(1) (a) Furuta, H.; Asano, T.; Ogawa, T. *J. Am. Chem. Soc.* **1994**, *116*, 767−768. (b) Chmielewski, P. J.; Latos-Grazynski, L.; Rachlewicz, K.; Glowiak, T. *Angew. Chem., Int. Ed. Engl.* **1994**, *33*, 779−781. (c) Srinivasan, A.; Furuta, H. *Acc. Chem. Res.* **2005**, *38*, 10−20. (d) Toganoh, M.; Furuta, H. *Chem. Commun.* **2012**, *48*, 937−954.

(2) (a) Lash, T. D. In *The Porphyrin Handbook*; Kadish, K. M., Smith, K. M., Guilard, R., Eds.; Academic Press: San Diego, CA, 2000; Vol. 2, pp 125−199. (b) Lash, T. D. *Eur. J. Org. Chem.* **2007**, *2007*, 5461−5481.

(3) Lash, T. D. In *Handbook of Porphyrin Science—With Applications to Chemistry, Physics, Material Science, Engineering, Biology and Medicine*; Kadish, K. M., Smith, K. M., Guilard, R., Eds.; World Scientific Publishing: Singapore, 2012; Vol. 16, pp 1−329.

(4) Lash, T. D. *Org. Biomol. Chem.* **2015**, *13*, 7846−7878.

(5) (a) Lash, T. D. *Angew. Chem., Int. Ed. Engl.* **1995**, *34*, 2533−2535. (b) Lash, T.D.; Chaney, S. T.; Richter, D. T. *J. Org. Chem.* **1998**, *63*, 9076−9088.

(6) (a) Lash, T. D.; Hayes, M. J. *Angew. Chem., Int. Ed. Engl.* **1997**, *36*, 840−842. (b) Lash, T. D.; Hayes, M. J.; Spence, J. D.; Muckey, M. A.; Ferrence, G. M.; Szczepura, L. F. *J. Org. Chem.* **2002**, *67*, 4860−4874. (c) Li, D.; Lash, T. D. *J. Org. Chem.* **2014**, *79*, 7112−7121.

(7) (a) Lash, T. D.; Chaney, S. T. *Tetrahedron Lett.* **1996**, *37*, 8825−8828. (b) Bergman, K. M.; Ferrence, G. M.; Lash, T. D. *J. Org. Chem.* **2004**, *69*, 7888−7897.

(8) Lash, T. D.; Chaney, S. T. *Angew. Chem., Int. Ed. Engl.* **1997**, *36*, 839−840.

(9) Lash, T. D. *Chem. - Asian J.* **2014**, *9*, 682−705.

(10) Harvey, J. D.; Ziegler, C. J. *Coord. Chem. Rev.* **2003**, *247*, 1−19.

(11) Chmielewski, P. J.; Latos-Grazynski, L. *Coord. Chem. Rev.* **2005**, *249*, 2510−2533.

(12) Toganoh, M.; Furuta, H. In *Handbook of Porphyrin Science—With Applications to Chemistry, Physics, Material Science, Engineering, Biology and Medicine*; Kadish, K. M., Smith, K. M., Guilard, R., Eds.; World Scientific Publishing: Singapore, 2010; Vol. 2, pp 103−192.

(13) Stepien, M.; Latos-Grazynski, L. *Acc. Chem. Res.* **2005**, *38*, 88−98.

(14) (a) Lash, T. D.; Rasmussen, J. M.; Bergman, K. M.; Colby, D. A. *Org. Lett.* **2004**, *6*, 549−552. (b) Lash, T. D.; Young, A. M.; Rasmussen, J. M.; Ferrence, G. M. *J. Org. Chem.* **2011**, *76*, 5636−5651.

(15) (a) Muckey, M. A.; Szczepura, L. F.; Ferrence, G. M.; Lash, T. D. *Inorg. Chem.* **2002**, *41*, 4840−4842. (b) Lash, T. D.; Colby, D. A.; Szczepura, L. F. *Inorg. Chem.* **2004**, *43*, 5258−5267. (c) Lash, T. D. *Org. Lett.* **2011**, *13*, 4632−4635.

(16) (a) Young, A. M.; Von Ruden, A. L.; Lash, T. D. *Org. Biomol. Chem.* **2011**, *9*, 6293−6305. (b) Li, R.; Lammer, A. D.; Ferrence, G. M.; Lash, T. D. *J. Org. Chem.* **2014**, *79*, 4078−4093.

(17) Lash, T. D.; Colby, D. A.; Graham, S. R.; Chaney, S. T. *J. Org. Chem.* **2004**, *69*, 8851−8864.

(18) Lash, T. D.; El-Beck, J. A.; Ferrence, G. M. *J. Org. Chem.* **2007**, *72*, 8402−8415.

(19) Lash, T. D. *Chem. Commun.* **1998**, 1683−1684.

(20) Graham, S. R.; Ferrence, G. M.; Lash, T. D. *Chem. Commun.* **2002**, 894−895.

(21) Lash, T. D.; Colby, D. A.; Graham, S. R.; Ferrence, G. M.; Szczepura, L. F. *Inorg. Chem.* **2003**, *42*, 7326−7338.

(22) Lash, T. D.; Pokharel, K.; Zeller, M.; Ferrence, G. M. *Chem. Commun.* **2012**, *48*, 11793−11795.

(23) Stateman, L. M.; Ferrence, G. M.; Lash, T. D. *Organometallics* **2015**, *34*, 3842−3848.

(24) Graham, S. R.; Colby, D. A.; Lash, T. D. *Angew. Chem., Int. Ed.* **2002**, *41*, 1371−1374.

(25) Lash, T. D.; Lammer, A. D.; Idate, A. S.; Colby, D. A.; White, K. *J. Org. Chem.* **2012**, *77*, 2368−2381.

(26) Colby, D. A.; Lash, T. D. *Chem. - Eur. J.* **2002**, *8*, 5397−5402.

(27) Lash, T. D.; Colby, D. A.; Ferrence, G. M. *Eur. J. Org. Chem.* **2003**, *2003*, 4533−4548.

(28) El-Beck, J. A.; Lash, T. D. *Eur. J. Org. Chem.* **2007**, *2007*, 3981−3990.

(29) Bialek, M. J.; Latos-Grazynski, L. *Chem. Commun.* **2014**, *50*, 9270−9272.

(30) Colby, D. A.; Ferrence, G. M.; Lash, T. D. *Angew. Chem., Int. Ed.* **2004**, *43*, 1346−1349.

(31) Bialek, M. J.; Bialonska, A.; Latos-Grazynski, L. *Inorg. Chem.* **2015**, *54*, 6184−6194.

(32) Stepien, M.; Latos-Grazynski, L. *Chem. - Eur. J.* **2001**, *7*, 5113−5117.

(33) Lash, T. D.; Szymanski, J. T.; Ferrence, G. M. *J. Org. Chem.* **2007**, *72*, 6481−6492.

(34) Young, A. M.; Lash, T. D. *Org. Biomol. Chem.* **2013**, *11*, 6841−6848.

(35) Lash, T. D.; Lammer, A. D.; Idate, A. S.; Colby, D. A.; White, K. *J. Org. Chem.* **2012**, *77*, 2368−2381.

(36) Because of an instrument malfunction, the previously reported λ_{max} values of **14a** are incorrect.[30] This mistake was not recognized at the time but did not lead to any further errors in related studies.

(37) (a) Ghosh, A. In *The Porphyrin Handbook*; Kadish, K. M., Smith, K. M., Guilard, R., Eds.; Academic Press: San Diego, CA, 2000; Vol. 7, pp 1−38. (b) Ghosh, A.; Wondimagegn, T.; Nilsen, H. J. *J. Phys. Chem. B* **1998**, *102*, 10459−10467. (c) Ghosh, A. *Acc. Chem. Res.* **1998**, *31*, 189−198.

(38) Zhao, Y.; Truhlar, D. G. *Theor. Chem. Acc.* **2008**, *120*, 215−241.

(39) Grimme, S. *J. Comput. Chem.* **2004**, *25*, 1463−1473.

(40) AbuSalim, D. I.; Lash, T. D. *Org. Biomol. Chem.* **2014**, *12*, 8719−8736.

(41) Toganoh, M.; Furuta, H. *J. Org. Chem.* **2013**, *78*, 9317−9327.

(42) AbuSalim, D. I.; Ferrence, G. M.; Lash, T. D. *J. Am. Chem. Soc.* **2014**, *136*, 6763−6772.

(43) Schleyer, P. v. R.; Maerker, C.; Dransfeld, A.; Jiao, H.; Hommes, N. J. R. v. E. *J. Am. Chem. Soc.* **1996**, *118*, 6317−6318.

(44) Corminboeuf, C.; Heine, T.; Seifert, G.; Schleyer, P. v. R.; Weber, J. *Phys. Chem. Chem. Phys.* **2004**, *6*, 273−276.

(45) Fallah-Bagher-Shaidaei, H.; Wannere, C. S.; Corminboeuf, C.; Puchta, R.; Schleyer, P. v. R. *Org. Lett.* **2006**, *8*, 863−866.

(46) Mills, N. S.; Llagostera, K. B. *J. Org. Chem.* **2007**, *72*, 9163−9169.

(47) Solà, M.; Feixas, F.; Jiménez-Halla, J. O. C.; Matito, E.; Poater, J. *Symmetry* **2010**, *2*, 1156−1179.

(48) Geuenich, D.; Hess, K.; Kohler, F.; Herges, R. *Chem. Rev.* **2005**, *105*, 3758−3772.

(49) Clezy, P. S. In *The Porphyrins*; Dolphin, D., Ed.; Academic Press: New York, 1978; Vol. *II*, p 103.

(50) Senge, M. O.; Smith, K. M. *J. Chem. Soc., Chem. Commun.* **1992**, 1108−1109.

(51) Hung, C.-H.; Wang, S.-L.; Ko, J.-L.; Peng, C.-H.; Hu, C.-H.; Lee, M.-T. *Org. Lett.* **2004**, *6*, 1393−1396.

(52) Bruno, I. J.; Cole, J. C.; Kessler, M.; Luo, J.; Motherwell, W. D. S.; Purkis, L. H.; Smith, B. R.; Taylor, R.; Cooper, R. I.; Harris, S. E.; Orpen, A. G. *J. Chem. Inf. Model.* **2004**, *44*, 2133−2144.

(53) Stepien, M.; Latos-Grazynski, L. *Inorg. Chem.* **2003**, *42*, 6183−6193.

(54) Cyrañski, M. K.; Krygowski, T. M.; Wisiorowski, M.; van Eikema Hommes, N. J. R.; Schleyer, P. v. R. *Angew. Chem., Int. Ed.* **1998**, *37*, 177−180.

(55) Ferrence, G. M.; Lash, T. D. *Acta Crystallogr., Sect. E: Struct. Rep. Online* **2007**, *63*, m1351−m1353.

(56) Zhang, Z.; Ferrence, G. M.; Lash, T. D. *Org. Lett.* **2009**, *11*, 101−104.

(57) Bondi, A. *J. Phys. Chem.* **1964**, *68*, 441−451.

(58) Groom, C. R.; Allen, F. H. *Angew. Chem., Int. Ed.* **2014**, *53*, 662−671.

(59) Frisch, M. J.; Trucks, G. W.; Schlegel, H. B.; Scuseria, G. E.; Robb, M. A.; Cheeseman, J. R.; Scalmani, G.; Barone, V.; Mennucci, B.; Petersson, G. A.; Nakatsuji, H.; Caricato, M.; Li, X.; Hratchian, H. P.; Izmaylov, A. F.; Bloino, J.; Zheng, G.; Sonnenberg, J. L.; Hada, M.; Ehara, M.; Toyota, K.; Fukuda, R.; Hasegawa, J.; Ishida, M.; Nakajima, T.; Honda, Y.; Kitao, O.; Nakai, H.; Vreven, T.; Montgomery, J. A., Jr.; Peralta, J. E.; Ogliaro, F.; Bearpark, M.; Heyd, J. J.; Brothers, E.; Kudin, K. N.; Staroverov, V. N.; Kobayashi, R.; Normand, J.; Raghavachari, K.; Rendell, A.; Burant, J. C.; Iyengar, S. S.; Tomasi, J.; Cossi, M.; Rega, N.; Millam, N. J.; Klene, M.; Knox, J. E.; Cross, J. B.; Bakken, V.; Adamo, C.; Jaramillo, J.; Gomperts, R.; Stratmann, R. E.; Yazyev, O.; Austin, A. J.; Cammi, R.; Pomelli, C.; Ochterski, J. W.; Martin, R. L.; Morokuma, K.; Zakrzewski, V. G.; Voth, G. A.; Salvador, P.; Dannenberg, J. J.; Dapprich, S.; Daniels, A. D.; Farkas, Ö.; Foresman, J. B.; Ortiz, J. V.; Cioslowski, J.; Fox, D. J. *Gaussian 09*, Revision D.01; Gaussian, Inc: Wallingford, CT, 2009.

(60) Wolinski, K.; Hinton, J. F.; Pulay, P. *J. Am. Chem. Soc.* **1990**, *112*, 8251−8260.

(61) Herges, R.; Geuenich, D. *J. Phys. Chem. A* **2001**, *105*, 3214−3220.